



Synthesis of SiC nanoparticles by SHG 532 nm Nd:YAG laser ablation of silicon in ethanol

Khawla S. Khashan¹ · Raid A. Ismail¹ · Rana O. Mahdi¹

Received: 28 February 2018 / Accepted: 4 May 2018 / Published online: 23 May 2018
© Springer-Verlag GmbH Germany, part of Springer Nature 2018

Abstract

In this work, colloidal spherical nanoparticles NPs of silicon carbide SiC have been synthesized using second harmonic generation 532 nm Nd:YAG laser ablation of silicon target dipped in ethanol solution at various laser fluences (1.5–5) J/cm². X-Ray diffraction XRD, scanning electron microscopy SEM, transmission electron microscope TEM, Fourier transformed infrared spectroscopy FT-IR, Raman spectroscopy, photoluminescence PL spectroscopy, and UV–Vis absorption were employed to examine the structural, chemical and optical properties of SiC NPs. XRD results showed that all synthesised SiC nanoparticles are crystalline in nature and have hexagonal structure with preferred orientation along (103) plane. Raman investigation showed three characteristic peaks 764, 786 and 954 cm⁻¹, which are indexing to transverse optic TO phonon mode and longitudinal optic LO phonon mode of 4H-SiC structure. The optical absorption data showed that the values of optical energy gap of SiC nanoparticles prepared at 1.5 J/cm² was 3.6 eV and was 3.85 eV for SiC synthesised at 5 J/cm². SEM investigations confirmed that the nanoparticles synthesised at 5 J/cm² are agglomerated to form larger particles. TEM measurements showed that SiC particles prepared at 1.5 J/cm² have spherical shape with average size of 25 nm, while the particles prepared at 5 J/cm² have an average size of 55 nm.

1 Introduction

Silicon carbide SiC is promising wide band gap semiconducting material which exhibits superior and attractive properties such as high breakdown field strength, high chemical stability, high thermal conductivity, outstanding resistance to oxidation and corrosion, and extreme hardness. These semiconductors have been used widely in various applications that require high temperature and high frequency such as light emitting diodes and UV detectors. Synthesis of one-dimensional 1D nanostructured SiC draws attention due to the unique properties which make it a candidate to be used in optical applications and nanoblocks in high-power semiconductor devices operating in cruel ambient [1]. Many methods have been employed for preparing SiC nanocrystals such as vapor–liquid–solid, vapor solid, chemical vapor deposition CVD, sol–gel, and decomposition of organic silicon compound laser ablation [2–7]. Among them, pulsed Laser Ablation in Liquid (PLAL) technique has significantly emerged

in the past years. PLAL technique is considered a well-established approach for the synthesizing and commercialization of colloidal nanoparticles [8]. PLAL has many advantages over the other conventional methods; it is a clean synthesis process, simple, cost-effective, it does not need chemical precursors and reducing agents, resulting in highly pure and stable nanoparticles; it is carried out at low temperature, gives opportunity to further nanoscale manipulations [9, 10]. Attempts of controlling the properties of nanoparticles (particle size and distribution) synthesised by laser ablation was carried out via selecting the appropriate parameters such as wavelength, pulse width, laser fluence, ablation time and liquid type [11, 12]. Yang et al. reported the preparation of nanocrystalline diamond by laser ablation of graphite target in water [13]. Liu et al. synthesised micro- and nanocubes of carbon with C8-like structure by laser ablation in liquid [14]. Kuzmin et al. [15] investigated the size control and optical properties of silicon nanoparticles prepared by femtosecond laser ablation of silicon nanoparticles in ethanol and they revealed that laser ablation of silicon target in methanol resulted in poorly oxidized silicon particles. Xiao et al. [16] demonstrated the possibility of reversible nanodiamond-carbon onion phase transformation by laser irradiation of colloidal suspensions of nanodiamonds at ambient temperature

✉ Khawla S. Khashan
khawla_salah@yahoo.com

¹ Department of Applied Science, University of Technology, Baghdad, Iraq

and pressure. The effect of applying external electric field on properties of nanomaterials prepared by laser ablation in liquid has been reviewed by Xiao et al. [17]. Few data were reported on the laser ablation of SiC nanoparticles [18–20] and the control on their properties and further investigation on the synthesis mechanism are still required. Recently, we have reported on the preparation of high photosensitivity nanostructured 4H-SiC/Si heterojunction by 1064 nm Nd:YAG laser ablation of silicon target in ethanol [21]. One of the alternative suggested approaches to control the size and distribution of synthesised nanoparticles was variation of the laser parameters such as laser wavelength, pulse width and laser fluence. Here, we reported the synthesis SiC nanoparticles by 532 nm nanosecond Nd:YAG laser ablation of silicon target in ethanol under different laser fluences without using any catalyst.

2 Experimental

Silicon carbide nanoparticles were produced by laser ablation of high purity 99.99% silicon target placed in the bottom of quartz vessel filled with 3 ml of pure ethanol. The colloidal solutions were synthesised by irradiating of Si target with second harmonic of Nd:YAG laser pulses operating at $\lambda = 532$ nm (type HUAFEL) with pulse duration of 7 ns and 1 Hz repetition. The laser fluences used for ablation were in the range of (1.5–5) J/cm^2 and the ablation time was 15 min for all samples. The laser beam was focused on the target surface using positive lens of 80 mm focal length. The spot size of laser beam on target was measured and found to be 2 mm. The laser energy reached the surface of the target was measured with Joule meter after taking into account the transmission of ethanol at 532 nm. The schematic diagram of experimental set up of laser ablation system used in this study is given in Fig. 1. The XRD data were obtained on a

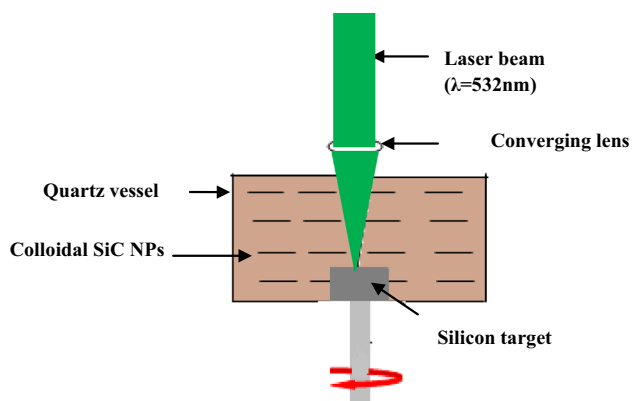


Fig. 1 Schematic diagram of experimental set-up of pulsed laser ablation of SiC NPs

(XRD-6000, Shimadzu X-ray diffractometer) using Cu K α X-ray source ($\lambda = 0.154056$ nm).

The morphology of SiC nanoparticles was examined using scanning electron microscopy (SEM Image Library) and transmission electron microscopy TEM (type CM10 pw 6020, Philips-Germany). The optical absorption of colloidal nanoparticles was studied with the aid of double-beam UV–Vis spectrophotometer model (shimadzu-1800). Photoluminescence PL measurements were carried out on spectrometer (Jobin Yvon model HR 800 Kyoto, Japan) at room temperature using Argon-ion laser ($\lambda = 244$ nm) as excitation source. Atomic force microscopy AFM (AA 3000) was used to investigate the morphology of nanoparticles. Fourier transformation infrared spectroscopy FT-IR (Bruker-7613) was used to investigate the chemical structure of the SiC NPs. Phase identification was investigated using Raman spectroscopy (Ranisaw RM1000 Raman spectrometer). Hall measurements were carried out at room temperature after making electrodes on SiC layer deposited on glass substrate using special masks.

3 Results and discussion

Figure 2 plots mass concentration of SiC NPs as function of laser fluence with error bars. We have found that increasing the laser fluence resulted in increasing the concentration of particles arising from increasing the quantity of ablated SiC particles since the laser beam with higher energy penetrates deeply inside the silicon target and resulting large ablated volume.

The XRD pattern of SiC NPs synthesised at laser fluence of 1.5 J/cm^2 has three peaks located at $2\theta = 28.8^\circ$, 37.56° and 43.9° corresponding to (111), (102) and (103) planes, respectively, is shown in Fig. 3. The first peak can be indexed to silicon resulted from the substrate, while the other two peaks are belonging to hexagonal structure 4H-SiC according to (JCPDS card #27-1402). No shift in diffraction peaks

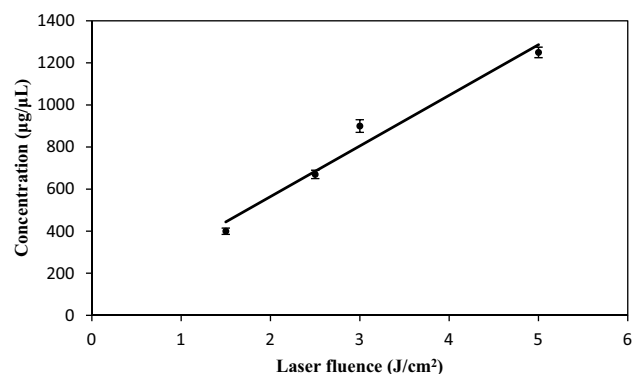


Fig. 2 Variation of particles concentration with laser fluence

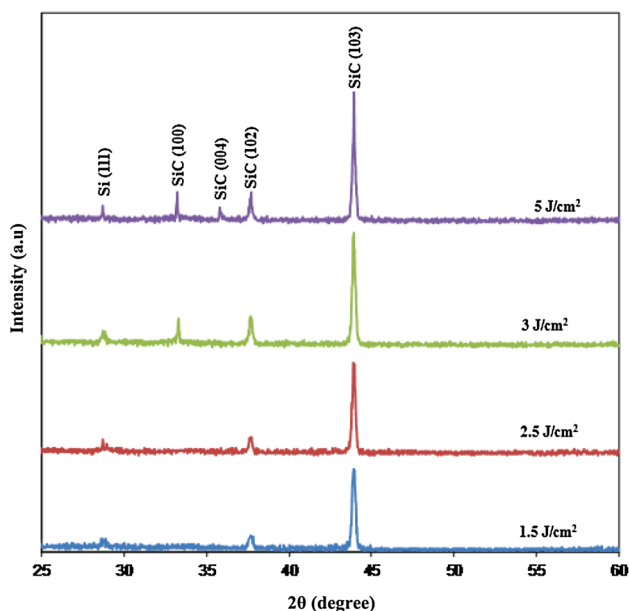


Fig. 3 XRD pattern for SiC NPs prepared at various laser fluences

was noticed after increasing the laser fluence to 2.5 J/cm², but when laser fluence increases to 3 J/cm², a new diffraction peak centered at 33.25° appeared in XRD spectrum which is related to 4H-SiC phase. On the other hand, the intensity of diffraction peak along (103) plane increases as laser fluence increases due to increasing particle size and concentration [22]. We note that further increase in the laser fluence resulted in appearance of another diffraction peak centered at 35.89° oriented along (004) plane which indexed to 4H-SiC phase. No other phases were observed in XRD patterns of SiC NPs. The *d* values of all diffraction peaks related to 4H-SiC NPs prepared at different laser fluences are given in Table 1. The average crystallite size (*D*) of SiC NPs was calculated using Scherrer’s formula [23].

$$D = \frac{0.9 \lambda}{\beta \cos(\theta)}, \tag{1}$$

where the β is the full width at the half maximum (FWHM) and λ is the X-ray wavelength. The average crystallite size of SiC NPs was decreased from 43.48 to 59.3 nm after increasing the laser fluence from 1.5 to 5 J/cm².

Figure 4 shows the SEM micrographs of the SiC NPs deposited on silicon substrate at different laser fluences. This figure confirmed formation of spherical and nanosized particles. For SiC nanoparticles synthesized with 1.5 J/cm², it was found that the average particle size was about 20 nm and agglomerated and aggregated particles were noticed as shown in Fig. 4. The concentration of SiC NPs was increased as laser fluence increases particularly for those prepared at 3 and 5 J/cm². With increase in the laser fluence to 5 J/cm², large SiC particles have formed (~60 nm) as depicted in

Fig. 4. The inset of Fig. 4 confirmed the formation of 4-H SiC crystalline phase which in good agreement with XRD results.

No remarkable difference in the values of particle size of SiC determined by SEM and XRD data. Figure 5 illustrates the 3D AFM images of SiC NPs synthesised at various laser fluences.

It is clearly seen that the morphology and particle size are laser fluence dependent, ablation at low laser fluence produces particles have spherical shape and uniform arranged over the entire layer. Increasing the laser fluence leads to formation pillar like particles oriented vertically and agglomerated particles were noticed. The SiC NPs prepared at high laser fluence exhibited different sized particles. As shown in Table 2, the average grain size was increased with increasing laser fluence; these results are in good agreement with those obtained from XRD results.

The particle size distribution was estimated from AFM investigation with the aid of software and given in Fig. 6. Narrow size distribution was noticed for SiC synthesised at 1.5 J/cm², it is in the range 58–100 nm. The particle size distribution for SiC NPs prepared at 5 J/cm² is nearly Gaussian type. Figure 7 demonstrates the TEM images and size histogram distribution of SiC NPs synthesized with different laser fluences. As shown in Fig. 6, the SiC NPs ablated at 1.5 J/cm² have quasi-spherical shapes and their sizes varied from 5 to 15 nm. Increasing the laser fluence to 2.5 J/cm² resulted in the production of the NPs with mean size approximately of 22 nm and aggregation of particles was clearly noticed.

The NPs prepared at 5 J/cm² were found to have mean size around 55 nm and the number of agglomerated particles produced at this condition was much larger than those of prepared at lower laser fluence. Figure 8 illustrates the photographs of SiC nanoparticles suspension which show gradient color from light brown yellow to dark brown yellow depending on laser fluence. The size of the nanoparticles and dielectric constant of the surrounding medium are affecting the color of the solution [24]. Figure 9 displays the optical absorption spectra of SiC nanoparticles prepared at various laser fluences. The absorption decreases sharply up to 400 nm and after this wavelength tends to saturate. The optical absorption of SiC NPs increases with laser fluence due to increasing the concentration of nanoparticles in solution.

The energy gap E_g of SiC NPs was estimated using Tauc’s relationship

$$\alpha h\nu = A(h\nu - E_g)^{0.5}, \tag{2}$$

where α is the absorption coefficient, *A* is constant and *hν* is the photon energy. The optical energy gap of SiC nanoparticles was determined from the plot of $(\alpha h\nu)^2$ versus *hν*, the intercept of the straight line with the *hν* axis gives the band gap as shown in Fig. 10. The optical energy gap was found

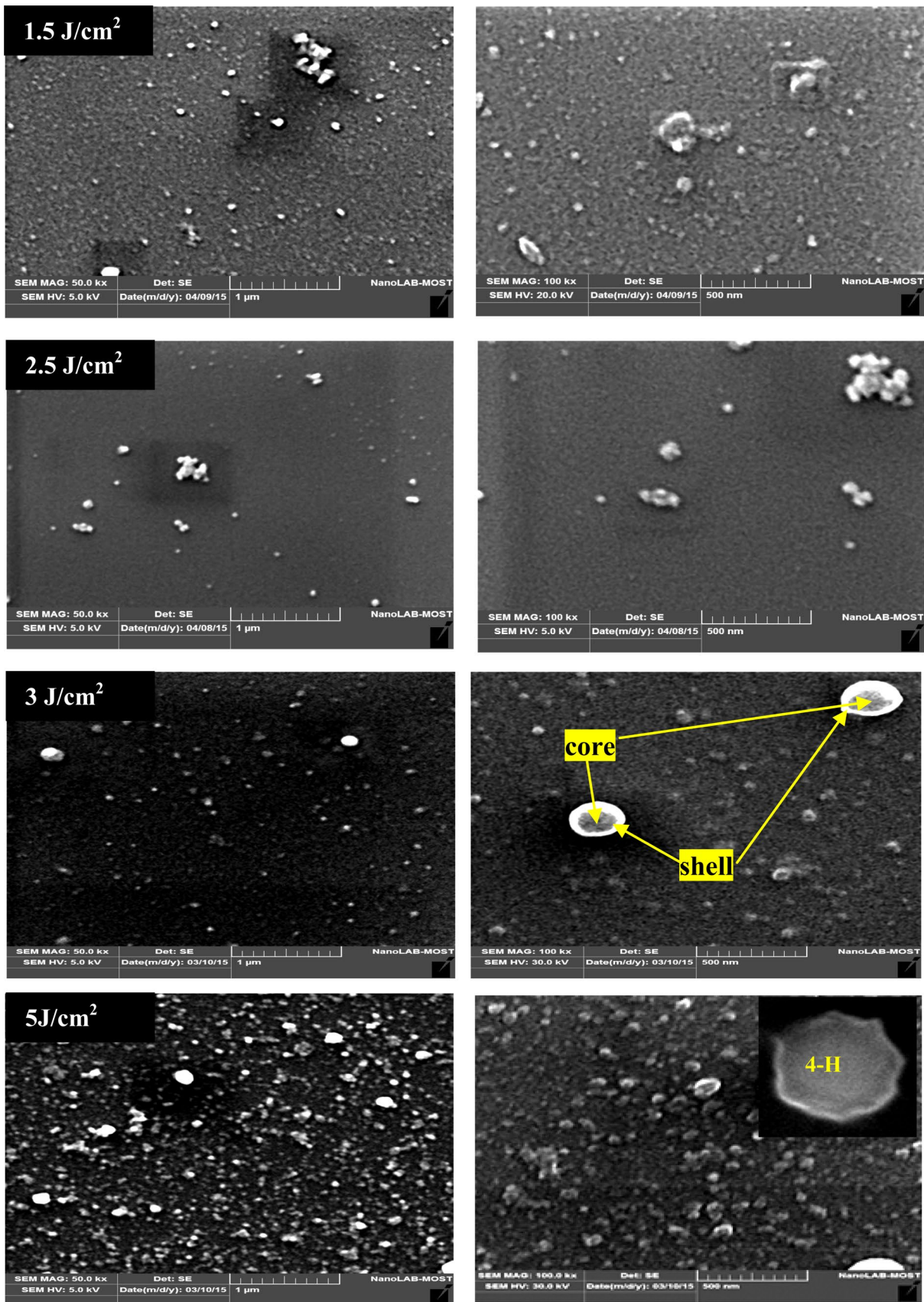


Fig. 4 SEM image of SiC NPs (left) and magnified SEM images (right) prepared at different laser fluences

Fig. 5 3D AFM images of SiC NPs

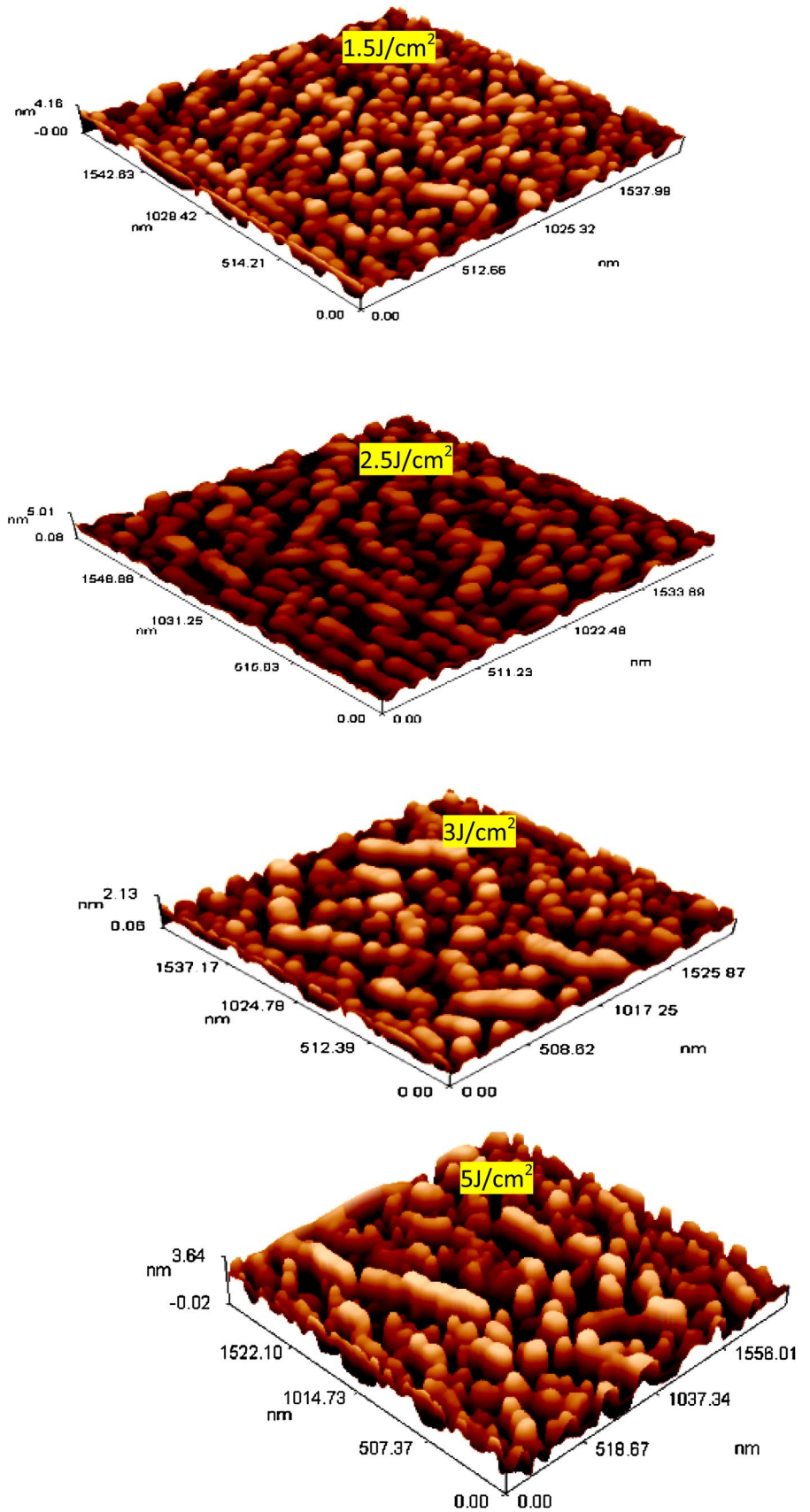


Table 1 Summary of XRD results for SiC NPs synthesised at various laser fluences

Laser fluences (J/cm ²)	2θ (deg)	hkl Plane	d Observed (Å)	d Standard (Å)	FWHM (deg)	D (nm)
1.5	37.65	(102)	2.387	2.352	0.1933	45.35
	43.9	(103)	2.06	2.084	0.2113	42.33
2.5	37.66	(102)	2.386	2.352	0.1733	50.55
	43.91	(103)	2.06	2.084	0.2159	41.43
3	33.29	(100)	2.688	2.661	0.151	57.35
	37.68	(102)	2.385	2.352	0.198	44.28
	43.91	(103)	2.06	2.084	0.2062	43.38
5	33.21	(100)	2.695	2.661	0.118	73.38
	35.83	(004)	2.503	2.513	0.14	62
	37.66	(102)	2.386	2.352	0.206	42.55
	43.91	(103)	2.06	2.084	0.2129	42

Table 2 Average grain size versus laser fluence

Laser fluence (J/cm ²)	Average grain size (nm)
1.5	55
2.5	66
3	74
5	78

in the range of (3.6–3.85) eV. The values of band gap are larger than those synthesised by 1064 nm laser pulses [21]. Blue shift was obtained for the particles prepared at low laser fluence due to the formation of small particles of SiC without particles agglomeration [25, 26]. Figure 11 shows that increasing the laser fluence leads to decrease in the optical band gap (SD = 0.02).

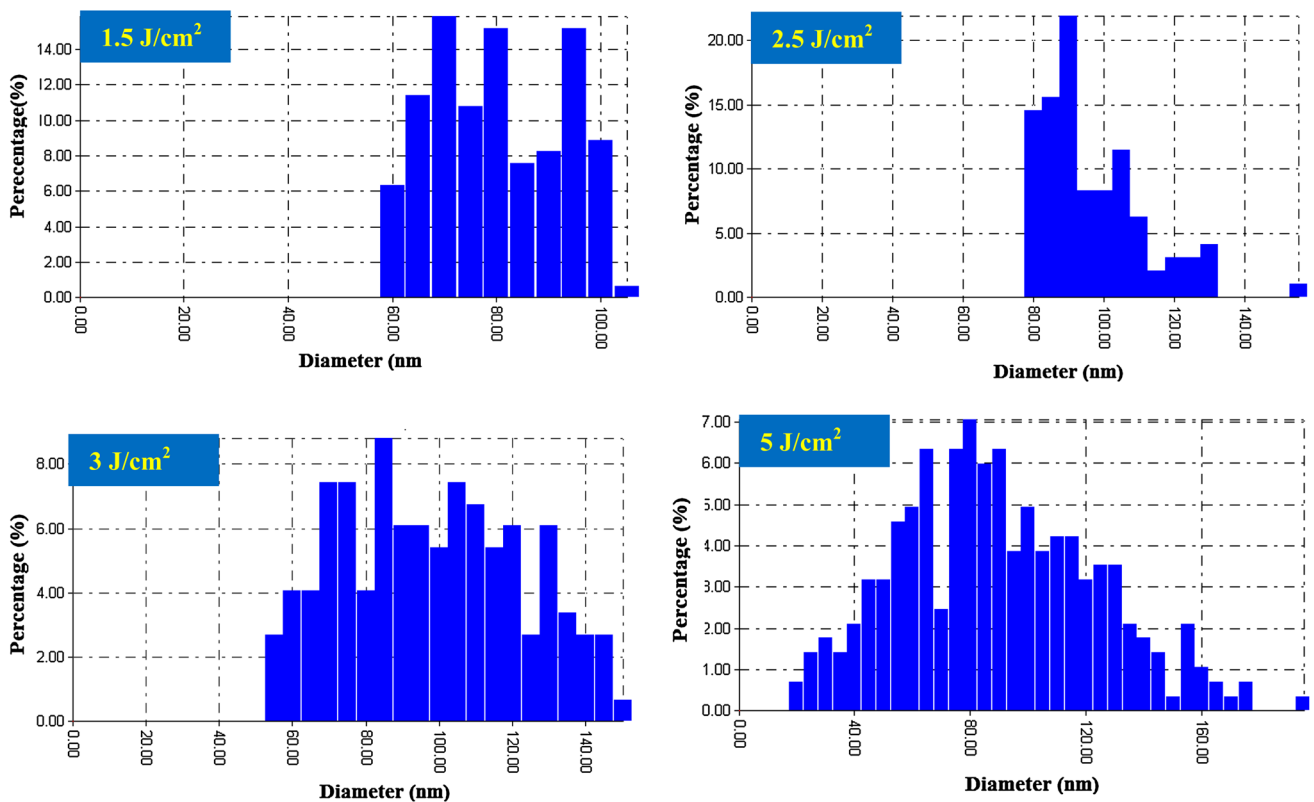


Fig. 6 Grain size distribution of SiC NPs prepared at various laser fluences

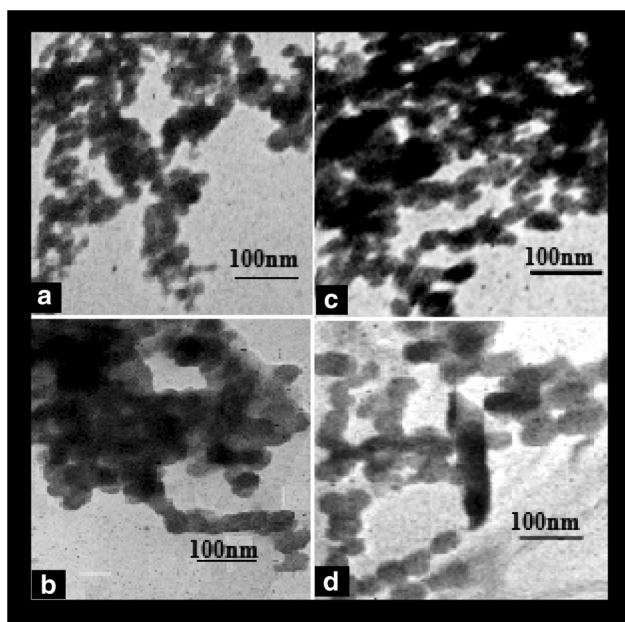


Fig. 7 TEM images and size distribution histograms of SiC colloidal nanoparticles prepared at a 1.5 J/cm², b 2.5 J/cm², c 3 J/cm², d 5 J/cm²

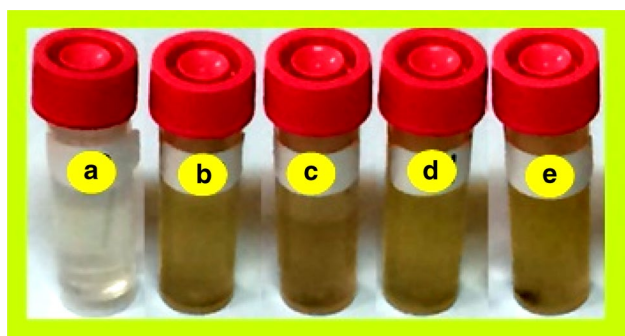


Fig. 8 Freshly colloidal SiC NPs prepared at different laser fluence. a Ethanol, b 1.5 J/cm², c 2 J/cm², d 3.5 J/cm², e 5 J/cm²

The room temperature photoluminescence of SiC NPs has been studied at excitation wavelength of 244 nm as shown in Fig. 12. The dominant PL emission was found to vary in position and in intensity both between SiC NPs samples with peak lying between 334 and 353 nm. A emission peak centered at 334 nm corresponding to 3.71 eV was detected for SiC NPs synthesised at 1.5 J/cm². Increasing the laser fluence shifts the emission peak to longer wavelength; this result can be attributed to quantum confinement effect and agrees with the results in Ref. [27]. The origin of emission peaks at 334, 340, 346 and 353 nm can be ascribed to band gap transitions within SiC NPs [28]. The intensity of PL spectra increased with increasing laser fluence due to increasing the concentration of SiC

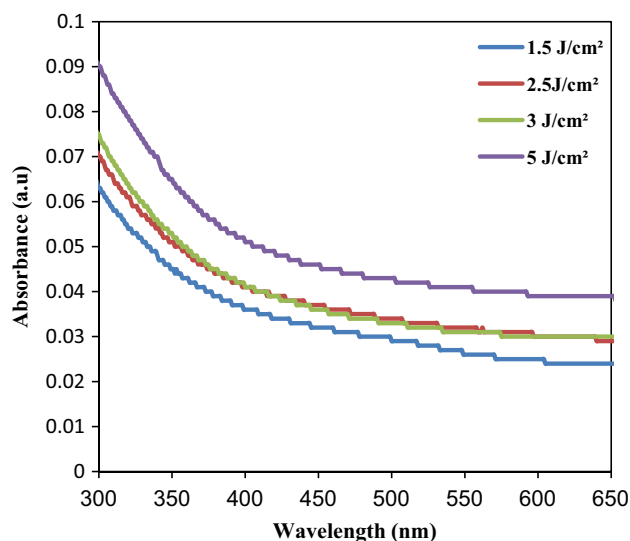


Fig. 9 Effect of laser fluence on the optical absorption of SiC NPs

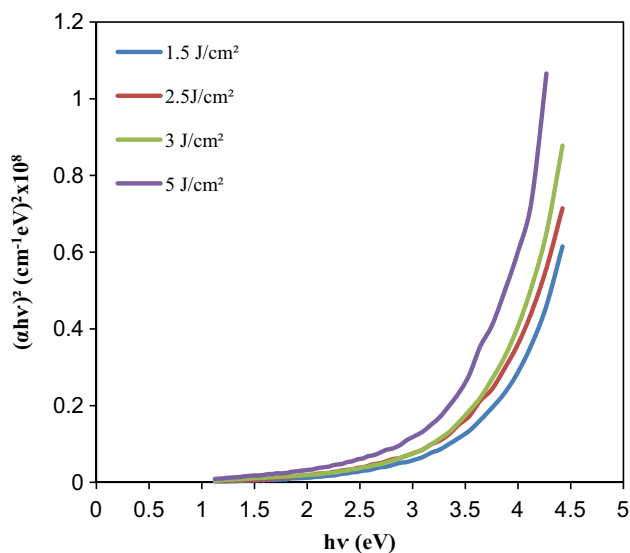


Fig. 10 $(\alpha h\nu)^2$ versus photon energy plot of SiC NPs prepared at different laser fluences

NPs [29]. No emission defect peaks have been observed in PL spectra.

Room temperature Raman spectra of SiC NPs synthesised at different laser fluences are given in Fig. 13. For SiC NPs prepared at 1.5 J/cm², three characteristic Raman peaks are observed at 764, 786 and 954 cm⁻¹ which can be indexed to the 4H-SiC phase. The first two peaks are transverse optic TO phonon modes with E_2 symmetry and the third Raman peak is longitudinal phonon LO mode with E_1 symmetry. These Raman peaks are shifted towards lower wavenumber compared to those prepared with 1064 nm Nd:YAG laser pulses. This mainly could be due to decrease in the particle

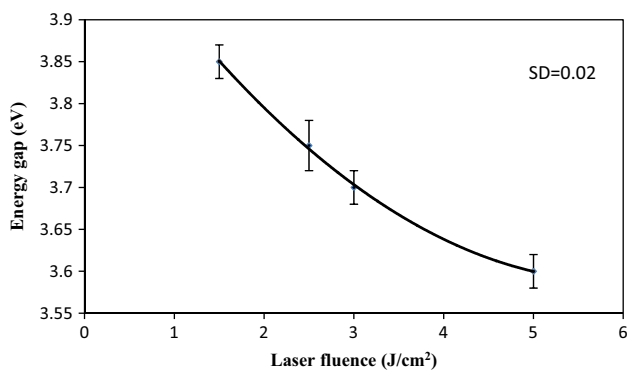


Fig. 11 Variation of optical energy gap with laser fluence

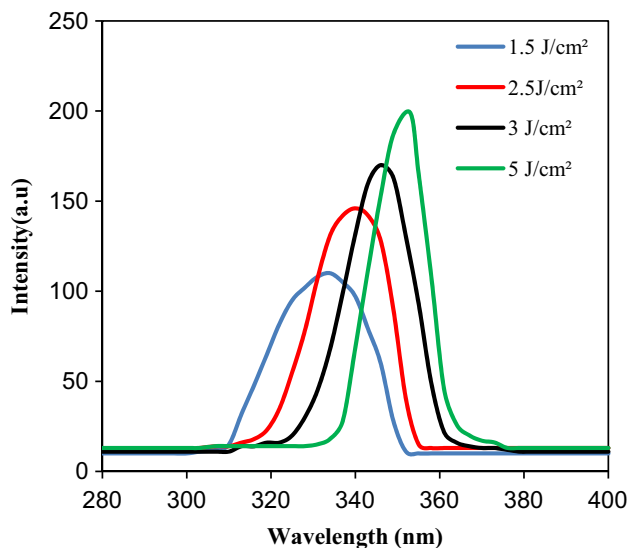


Fig. 12 Room temperature PL spectra of SiC NPs prepared at different laser fluences

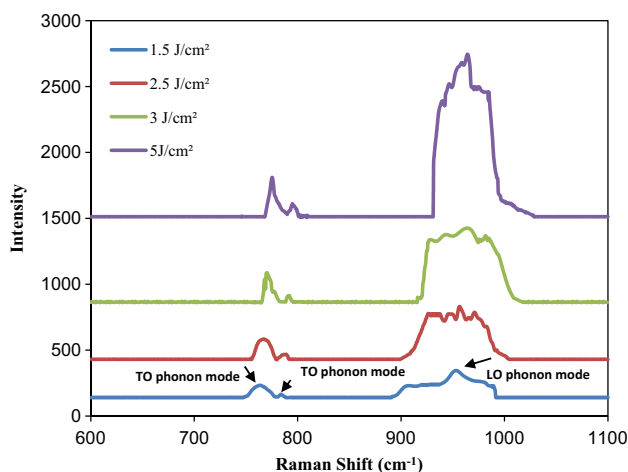


Fig. 13 Influence the laser fluence on the Raman spectra of SiC NPs

Table 3 Raman peaks of SiC NPs as a function of laser fluences

Laser fluence (J/cm ²)	Transverse optic mode TO (cm ⁻¹)	Transverse optic mode TO (cm ⁻¹)	Longitudinal optic mode LO (cm ⁻¹)
1.5	764	786	954
2.5	767	789	956
3	770	791	958
5	772	792	961

size, the SiC NPs prepared with 532 nm laser pulses exhibited smaller particles. By comparing the obtained peaks with the reported Raman peaks of bulk 4H-SiC structure [30, 31], the synthesised has frequency shift of 1–10 cm⁻¹ due to the structural defects created by laser pulses [32]. Increasing the laser fluence leads to increase in the intensity of Raman peaks, particularly the LO phonon mode also caused a shift in peaks toward higher frequency which probably attributes to increasing of the grain size and also due to internal stress [33]. Table 3 summarizes the phonon modes of 4H-SiC synthesised at different laser fluences observed by Raman investigation. The FT-IR spectra (transmission mode) of SiC NPs are shown in Fig. 14. Absorption peaks at 813, 814 and 816 cm⁻¹ are observed that assigned to SiC stretching vibration bond.

The absorption peaks at 876, 877, 878, 883, 886 and 888 cm⁻¹ are corresponding to bending vibration of the (Si-H) bond. The stretching vibration of (Si-O-Si) bond were observed at 1103, 1104, and 1105 cm⁻¹ and the peak at 1237 cm⁻¹ due to the bending vibration bond of (Si-CH₃). The absorption peak centered at 1459 cm⁻¹ can be related to the bending vibration of (CH₃) bond isolated from the ethanol environment. Furthermore the band observed at 1731, 2106 and 2333 cm⁻¹ was related to stretching vibration of (C=O) bond, symmetry stretching (C≡C) bond and (CO₂) vibration bond, respectively (Table 4). No significant effect of laser fluence on the position of absorption peaks was observed. Figure 15 shows the mobility and the electrical resistivity with error bars versus laser fluences of SiC NPs. It is clearly seen that the mobility increases as laser fluence increases due to the formation of larger SiC particles size (size dependent). The values of mobility are in good agreement with the results reported in Ref. [28]. Electrical resistivity as high as 10⁵ Ω cm was noticed for 4H-SiC prepared at 1.5 J/cm² which is very close to its intrinsic properties. The electrical resistivity was noticed dependent on laser fluence; it decreases from 6 × 10⁵ to 1.9 × 10² Ω cm as laser fluence increases from 1.5 to 5 J/cm², and this remarkable decrease in the electrical resistivity can be ascribed to the increase of the particles concentration and electron mobility of SiC.

On the other hand, the improvement in crystallinity degree of SiC layer with increasing the laser fluence plays main role

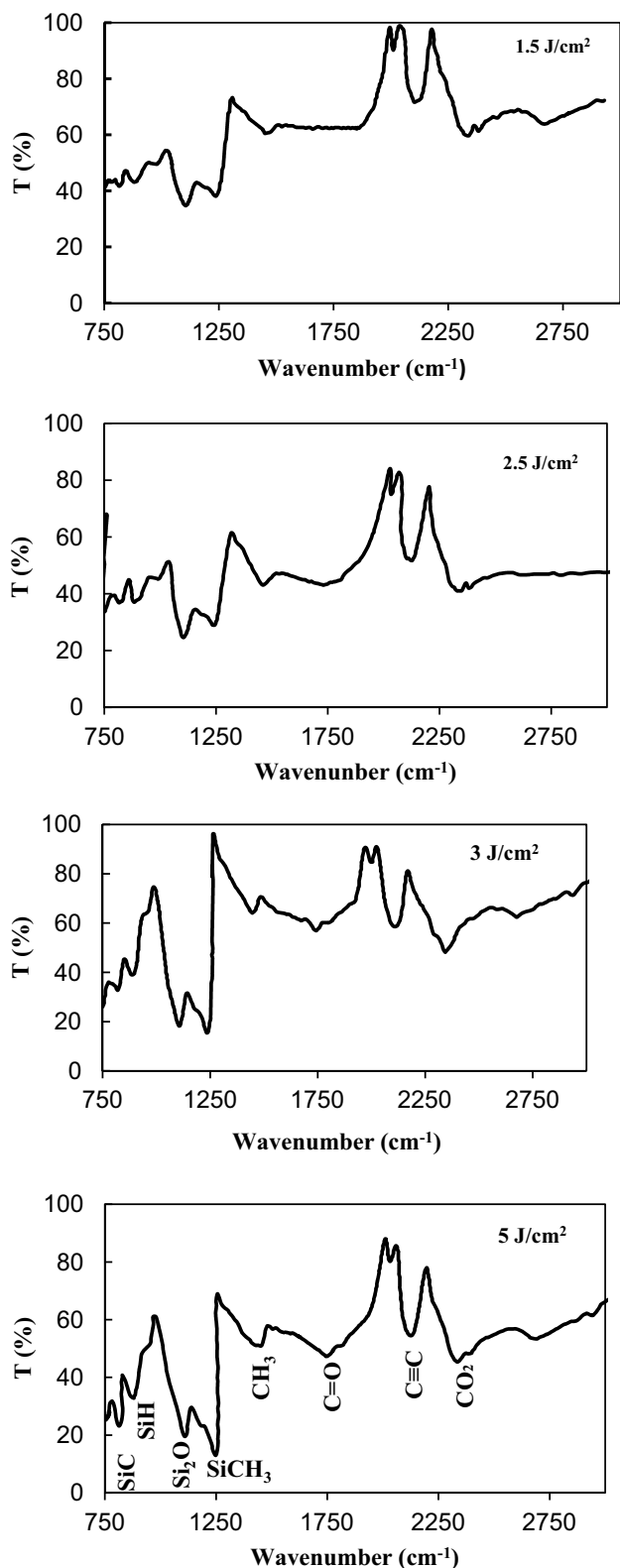


Fig. 14 FT-IR spectra of SiC NPs synthesised at various laser fluences

Table 4 Chemical bonds and their IR resonance position in SiC NPs

Observed bond value (cm ⁻¹)	Assignment	Vibration mode	References
813, 814, 816, 832, 835	Si-C	Stretching	[34, 35]
876, 877, 878, 880, 883, 884, 886, 0.888	Si-H	Bending	[34]
1103, 1104, 1105, 1100	Si-O-Si	Stretching	[34, 36]
1233, 1240, 1241	Si-CH ₃	Bending	[37, 38]
1450, 1451, 1453, 1459	CH ₃	Bending	[39]
1726, 1729, 1731, 1732	C=O	Stretching	[34]
2079, 2106, 2109, 2116	C≡C	Stretching	[39]
2333	CO ₂	Vibration	[18]

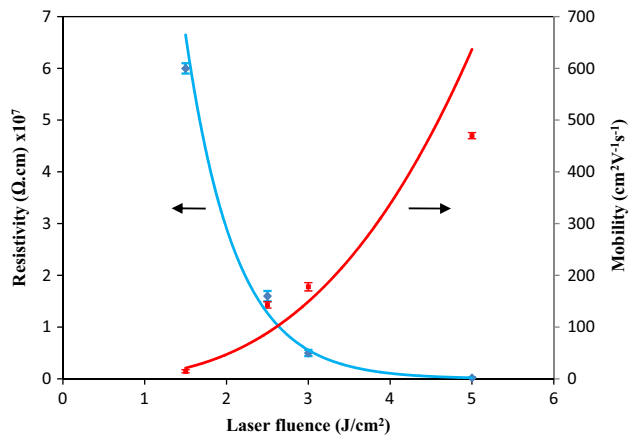


Fig. 15 Variation of electrical resistivity and electron mobility with laser fluence

in decreasing its electrical resistivity. The electrical resistivity and mobility are smaller than those of SiC NPs prepared at 1064 nm laser pulses reported in Ref. [21].

4 Conclusions

Simple and one-step synthesis of SiC nanoparticles was demonstrated using nanosecond laser ablation of high-purity Si wafer target in ethanol without using any catalyst. To control the properties of SiC particles, the laser fluence was varied from 1.5 to 5 J/cm². TEM and SEM findings revealed that the size, morphology and concentration of synthesised SiC nanoparticles can be controlled by selecting appropriate laser fluence. The nanoparticles concentration increases linearly with the laser fluence. The XRD investigations showed that the nanoparticles have highly crystalline 4H-SiC structure. Raman investigation confirmed the existence of three characteristic peaks which are related to transverse optic TO phonon mode and longitudinal optic LO phonon mode of 4H-SiC structure. PL data revealed that the dominant emission was found to vary in position and in intensity both between SiC NPs samples with peak lying between 334 and 353 nm. A blue shift was observed at laser fluence lower than 5 J/cm². The electron mobility and electrical resistivity of SiC NPs were changed remarkably with laser fluence. Based on the presented results and our previous data, the laser fluence and wavelength have significant role in manipulating the properties of SiC nanoparticles.

References

1. C. Weitzel, J. Palmour, C. Carter, K. Moore, K. Nordquist, S. Allen, C. Thero, M. Bhatnagar, *IEEE Trans. Electron. Device* **43**, 1732 (1996)
2. D. Tan, S. Zhou, J. Qiu, N. Khusroa, J. Photochem. Photobiol. C-Photochem. Rev **17**, 50 (2013)
3. H. Zeng, X.-W. Du, S. Singh, S. Kulinich, S. Yang, J. He, W. Cai, *Adv. Func. Mater.* **22**, 1333 (2012)
4. V. Amendola, M. Meneghetti, *Phys. Chem. Chem. Phys.* **15**, 3027 (2013)
5. H. Muto, K. Yamada, K. Miyajima, F. Mafun' e, *J. Phys. Chem. C* **111**, 17221 (2007)
6. S. Barcikowski, G. Compagnini, *Phys. Chem. Chem. Phys.* **15**, 3022 (2013)
7. S. Mhin, J. Ryu, K. Kim, G. Park, H. Ryu, K. Shim, T. Sasaki, N. Koshizaki, *Appl. Phys. A Mater. Sci. Process.* **96**, 435 (2009)
8. V. Amendola, M. Meneghetti, *Phys. Chem. Chem. Phys.* **11**, 3805 (2009)
9. R. Intartaglia, A. Barchanski, K. Bagga, A. Genovese, G. Das, P. Wagener, E. Fabrizio, A. Diaspro, F. Brandi, S. Barcikowski, *Nanoscale* **4**, 1271 (2012)
10. K. Bagga, A. Barchanski, R. Intartaglia, S. Dante, R. Marotta, A. Diaspro, C.L. Sajti, F. Brandi, *Laser Phys. Lett.* **10**, 065603 (2013)
11. J. Jeon, S. Yoon, H. Choi, J. Kim, D. Farson, S. Cho, *Appl. Sci.* **8**, 112 (2018)
12. M. Delmée, G. Mertz, J. Bardon, A. Marguier, L. Ploux, V. Roucoules, D. Ruch, *J. Phys. Chem. B* **121**, 6646 (2017)
13. G. Yang, J. Wang, Q. Liu, *J. Phys. Condens. Matter.* **10**, 35 (1998)
14. P. Liu, Y.L. Cao, C.X. Wang, X.Y. Chen, G.W. Yang, *Nano Lett.* **8**(8), 2570–2575 (2008)
15. P. Kuzmin, G. Shafeev, V. Bukin, et al. *J. Phys. Chem. C* **114**, 15266 (2010)
16. J. Xiao, G. Ouyang, P. Liu, C. Wang, G. Yang, *Nano Lett.* **14**(6), 3645 (2014)
17. J. Xiao, P. Liu, C.X. Wang, G.W. Yang, *Prog. Mater. Sci.* **87**, 140 (2017)
18. S. Yang, W. Cai, H. Zeng, X. Xu, *J. Mater. Chem.* **19**, 7119 (2009)
19. S. Yang, W. Cai, H. Zhang, H. Zeng, Y. Lei, *J. Phys. Chem. C* **115**, 7279 (2011)
20. S. Yang, B. Kiraly, W. Wang, S. Shang, B. Cao, H. Zeng, Y. Zhao, W. Li, Z. Liu, W. Cai, T. Huang, *Adv. Mater.* **24**, 5598 (2012)
21. K.R. Ismail, R. Khashan, R. Mahdi, *Mater. Sci. Semicond. Process* **68**, 252 (2017)
22. P. Lv, Z. Chen, A. Zhang, In: *Proceeding of the 2009 4th IEEE international conference on nano/micro engineering and molecular systems, 2009, China*
23. A.Y. Kamlag, I. Goossens, J. Schoonman, *Appl. Surf. Sci.* **184**, 118 (2001)
24. S. Eustis, PhD thesis, Georgia Institute of Technology, 2006, 1
25. S. Wageh, M. Maize, *J. Mater. Sci. Mater. Electron.* **25**, 4830 (2014)
26. W. Gong, Z. Zheng, J. Zheng, X. Hu, W. Gao, *J. Appl. Phys.* **102**, 64304 (2007)
27. R. Intartaglia, K. Bagga, M. Scotto, A. Diaspro, F. Brandi, *Opt. Mater. Express* **2**, 510 (2012)
28. R. Andrievski, *Rev. Adv. Mater. Sci.* **22**, 1 (2009)
29. Yu Zakharko, D. Rioux, S. Patskovsky, V. Lysenko, O. Marty, J. Bluet, M. Meunier, *Phys. Status Solidi RRL* **5**, 292 (2011)
30. T. Perova, J. Wasyluk, S. Kukushkin, A. Osipov, N. Feoktistov, S. Grudinlin, *Mater. Sci. Forum* **645**, 359 (2010)
31. S. Lin, Z. Chen, L. Li, C. Yang, *Mater. Res.* **15**, 833 (2012)
32. H. Zhang, W. Ding, K. He, M. Li, *Nanoscale Res. Lett.* **5**, 1264 (2010)

33. J. Zhu, W. Zhu, S. Nishino, G. Pezzotti, *Appl. Surf. Sci.* **252**, 2346 (2006)
34. M. Vennekaamp, I. Bauer, M. Groh, E. Sperling, S. Ueberlein, M. Myndy, K. Mader, S. Kaskel, *Beilstein J. Nanotechnol.* **2**, 665 (2011)
35. F. Han H. Zhu, N. Lun, Y. Qi, Y. Bai, J. Bi, X. Meng, B. Zhang, Y. Wang, J. Liuand, R. Fan, *J. Am. Ceram. Soc.* **93**, 2415 (2010)
36. X.C. Yang, W. Riehemann, H. Hofmeister, M. Dubiel, *Mater. Sci. Eng. B* **95**, 299 (2002)
37. P.J. Launer, *Silicon compound Register and review*, (Laboratory for Materials: Burnt Hills, New York, 1987)
38. G. Das, G. Mariotto, A. Quaranta, *J. Electrochem. Soc.* **153**, F46 (2006)
39. G. Lampman, D. Pavia, G. Kriz, *Introduction to organic spectroscopy*, (Macmillan, New York, 1987)